Underpotential Deposition of Te Monolayers on Au Surfaces from Perchloric Acid Solution Studied by Chronocoulometry and EQCM

Igor Nicic,[†] Jie Liang,[†] Vince Cammarata,[†] Murat Alanyalioglu,[‡] Umit Demir,*[,‡] and Curtis Shannon*[,†]

Department of Chemistry, Auburn University, Auburn, Alabama 36849-5312, and Department of Chemistry, Ataturk University, Erzurum, Turkey

Received: July 28, 2002; In Final Form: September 13, 2002

We report a study of the underpotential deposition (UPD) of Te monolayers onto Au electrodes from perchloric acid solution using electrochemical quartz microgravimetry (EQCM) and chronocoulometry. We find that tellurium(IV) oxide (as TeO_3^{2-}, TeO_2 or $HTeO_2^+$) is adsorbed onto Au at potentials positive of the UPD region. EQCM experiments, in which an Au electrode poised at +0.7 V in pure $HClO_4$ electrolyte was monitored as a function of time before and after the addition of TeO_2, showed a slow adsorption of a submonolayer of TeO_2. Energy-dispersive X-ray (EDX) measurements confirm the presence of a Te-containing species on the surface. Two distinct reductive UPD features at approximately +0.400 V and −0.100 V vs Ag|AgCl were observed by cyclic voltammetry. EQCM measurements indicate that there is a small, reproducible mass *decrease* accompanying the first UPD wave, consistent with the loss of H_2O from the surface as an adsorbed layer of $HTeO_2^+$ is reduced to a submonolayer of Te atoms. Chronocoulometry indicates a charge density of 160 $\mu C/cm^2$ for the first UPD wave, which, when taken together with the mass change data, is consistent with the four-electron reduction of adsorbed $HTeO_2^+$ to Te. In addition, analysis of the current−time data indicates that this process occurs by a two-dimensional instantaneous nucleation and growth mechanism, resulting in an ordered overlayer with a fractional coverage of ca. 0.41. The second UPD peak results in the formation of a dense monolayer by reduction of $HTeO_2^+$ from solution. This process also appears to occur by a direct four-electron reduction and exhibits simple Langmuir adsorption behavior as evidenced by exponentially decaying current−time transients. The saturation coverage is approximately 0.9.

Introduction

Thermal management issues have become increasingly important in the design of integrated circuits as well as lab-on-a-chip total analytical systems. This has generated renewed interest in the growth of thin film thermoelectric materials such as Bi_2Te_3, Sb_2Te_3, and PbTe. Electrodeposition (ED) is well-suited to the growth of telluride phases such as these because it can easily be integrated with other device fabrication technologies, is low cost, and can be carried out at room temperature.

A variety of schemes for the growth of telluride phases by ED have been reported. These include deposition into nanoporous templates,[1] deposition of thin films by electrochemical atomic layer epitaxy,[2] and electrochemical co-deposition of thin films and superlattices.[3] In an effort to better control the structural quality of the deposits that can be obtained, fundamental studies of the surface reactions, such as underpotential deposition (UPD), that are the basis of ED are an ongoing part of the development of new material growth cycles.

A significant number of studies on Te UPD have been reported.[4] Two UPD and two stripping waves are typically observed. Initially, Te nucleates and grows as a $(\sqrt{3} \times \sqrt{3})R30°$ structure with a high concentration of domain walls. The domain walls have a (13×13) periodicity that evolves into a structure with larger periodicity over time. Several other higher coverage structures, including $(\sqrt{7} \times \sqrt{13})R19.1°$ and (3×3) have also been observed. Finally, at more cathodic potentials, a high-coverage structure exists with a coverage of 0.9 ML. Nevertheless, several fundamental questions about this system remain unanswered. For example, it is still unresolved in the literature whether the Te precursor, typically TeO_2, is adsorbed onto the surface prior to the first UPD wave. Knowledge of the adsorption behavior of TeO_2 is important in developing a model for ED processes such as electrochemical atomic layer epitaxy (EC-ALE). It is well-known, for instance, that anions from the supporting electrolyte play an important role in the structure of many metallic UPD layers. Stickney and co-workers[5] have shown Auger electron spectroscopic evidence, obtained from ex situ electrochemistry−ultra-high-vacuum experiments, that an oxidized Te species is adsorbed at all positive potentials. Interestingly, neither an in situ SHG study[6] by Yagi et al. nor a recent in situ STM study by Hayden and co-workers[7] was able to resolve this issue unambiguously.

In this work, we employed in situ electrochemical quartz microgravimetry (EQCM) and chronoamperometry to study the UPD of Te onto Au surfaces from perchloric acid solutions in an effort to understand whether preadsorption of TeO_2 is an elementary step in the overall UPD mechanism. EQCM was able to directly probe the mass changes associated with each of the two UPD processes as well as the stripping peaks. Analysis of chronoamperometric current−time data provided

* To whom correspondence should be addressed. E-mail: shanncg@auburn.edu, phone 334-844-6964, fax 334-844-6959 (C.S.). E-mail: udemir@atauni.edu.tr, phone 90 442 231 4434, fax 90 442 236 0948 (U.D.).
[†] Auburn University.
[‡] Ataturk University.

10.1021/jp026625w CCC: $22.00
Published on Web 10/30/2002

information on the kinetics of two-dimensional nucleation and growth involved in monolayer formation/dissolution.

Experimental Section

Materials. TeO_2 (99.99% purity) was obtained from the Merck Chemical Company and used as received. Au wire (0.762 mm diameter, 99.999% purity) was obtained from Alfa Aesar. Millipore-Q purified distilled water was used to prepare all solutions.

Substrate Preparation. Au wire electrodes were cleaned by sequential rinsing with distilled water, absolute ethanol, piranha solution (1:3 v/v 30% H_2O_2, 18 M H_2SO_4), distilled water, and absolute ethanol. After being dried in a stream of flowing nitrogen, the clean Au wire was melted in a H_2/O_2 flame to form a 1.5−2.5 mm diameter droplet at the end of the wire. The droplet was annealed in the flame until numerous small Au(111) facets appeared across the surface of the polycrystalline droplet. Prior to all experiments, the Au electrodes were annealed in a H_2 flame for an additional 15 min.

Electrochemistry. All cyclic voltammetry experiments were performed in homemade single-compartment Teflon cells (ca. 20 mL total volume) using either a Cypress Systems Omni-101 or a BAS-100 workstation. A standard three-electrode configuration was used in which the Au bead was the working electrode, a Pt wire was the counter electrode, and Ag|AgCl was the reference electrode. All potentials are referenced to Ag|AgCl. The electrochemical cell was placed in a Faraday cage to isolate it from environmental electronic noise sources. Before and after transfer of the sample, the solution was thoroughly degassed with ultrapure Ar and was isolated from air with a blanket of Ar during experiments. The scan rate and geometric surface area of the working electrode are noted in each figure caption.

EQCM. Cyclic voltammetry experiments were performed on a modified AFRDE4 potentiostat (Pine Instrument Co.) with an EG&G PARC 175 programmer as an external analog signal. A National Instruments Lab PC+ DAQ board was used to trigger the programmer and simultaneously collect and digitize the data. A series of LabVIEW programs were written for data acquisition and storage. EQCM experiments were carried out with an ELCHEMA EQCN-601 nanobalance instrument, EQCN-603 remote probe unit, and EQCN-602 Faraday cage. A new 9.995-MHz polished quartz crystal electrode (QCE) (International Crystal Mfg. Co.) with 10 nm of Cr and 100 nm of Au was mounted to a 20-mL-volume cell with silicone glue and cured for at least 24 h. Before use, the new mounted cell was rinsed with fresh CH_2Cl_2. The keyhole-shaped electrode had an area of 0.22 cm^2. The solution was degassed with 99.999% Ar for 15 min in a Faraday cage. The reference electrode was Ag|AgCl saturated with KCl, and all potentials are quoted vs Ag|AgCl. The counter electrode was Pt gauze. All EQCM data are presented in terms of change of mass from the beginning of the voltammetry (Δmass) and are calculated from the frequency changes using the Sauerbrey equation.[8]

Results and Discussion

The cyclic voltammetric behavior of a Au(111) electrode in 0.25 mM TeO_2 in $HClO_4$ electrolyte is shown in Figure 1. The voltammogram is characterized by two cathodic (deposition) features, labeled C1 and C2, as well as two anodic (stripping) peaks, labeled A1 and A2. Electrochemical "window-opening" experiments, in which the cathodic and anodic switching potentials were systematically varied, demonstrate that peaks A1/C1 and A2/C2 are conjugate.

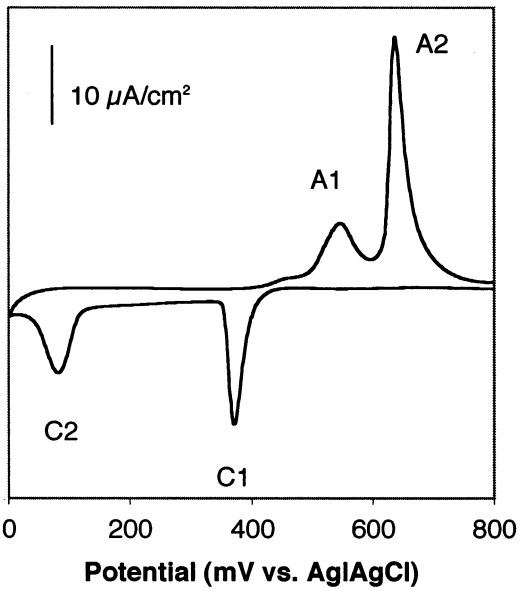

Figure 1. Cyclic voltammetry of a Au(111) electrode immersed in 0.25 mM TeO_2 in 0.10 M $HClO_4$ supporting electrolyte. Only the underpotential deposition (UPD) region is shown. The sweep rate was 0.100 V/s.

Peak C1. Chronocoulometry measurements indicate that there is a 160 $\mu C/cm^2$ faradaic charge associated with the first UPD peak (C1). In addition, potential step experiments through this peak show that it is associated with a 2D nucleation and growth event (Figure 2A). The kinetics of monolayer formation by two-dimensional nucleation and growth is now well understood.[9] We fit the experimental current−time data to the two limiting cases: instantaneous nucleation, when the nucleation rate is large and the maximum number of nuclei are formed upon stepping the potential, and progressive nucleation, when the nucleation rate is small and remains constant on the time scale of the experiment. Current density−time transients are described by the equations

$$j_{\text{inst}} = at\exp(-bt^2) \tag{1}$$

for the instantaneous case and

$$j_{\text{prog}} = ct^2\exp(-dt^3) \tag{2}$$

for the progressive case. The preexponential terms give the current density into the step edges of the expanding nuclei (i.e., the short-time behavior). The exponential terms correct for the decreased step edge length due to the overlap of adjacent nuclei at longer times. Explicit formulas for the constants *a*, *b*, *c*, and *d* can be found in the literature.[10] Experimental current−time transients were fit using so-called reduced variable plots following the procedure of Bewick, Fleischmann, and Thirsk.[11] The experimental potential step data and the corresponding reduced variable plots are shown in Figure 2A and 2B, respectively, and are characteristic of instantaneous growth kinetics. It is also clear from the potential step measurements that this process is quite rapid, occurring on the time scale of a few tens of milliseconds. To help determine the deposition mechanism, we carried out in situ EQCM measurements as the electrode potential was scanned through peak C1. These data are shown in Figure 3. Interestingly, there is a very reproducible mass *decrease* associated with this UPD feature, although the mass change is small, ca. 10 ng for a 0.255 cm^2 surface area electrode. The fact that the mass change is negative and initiates

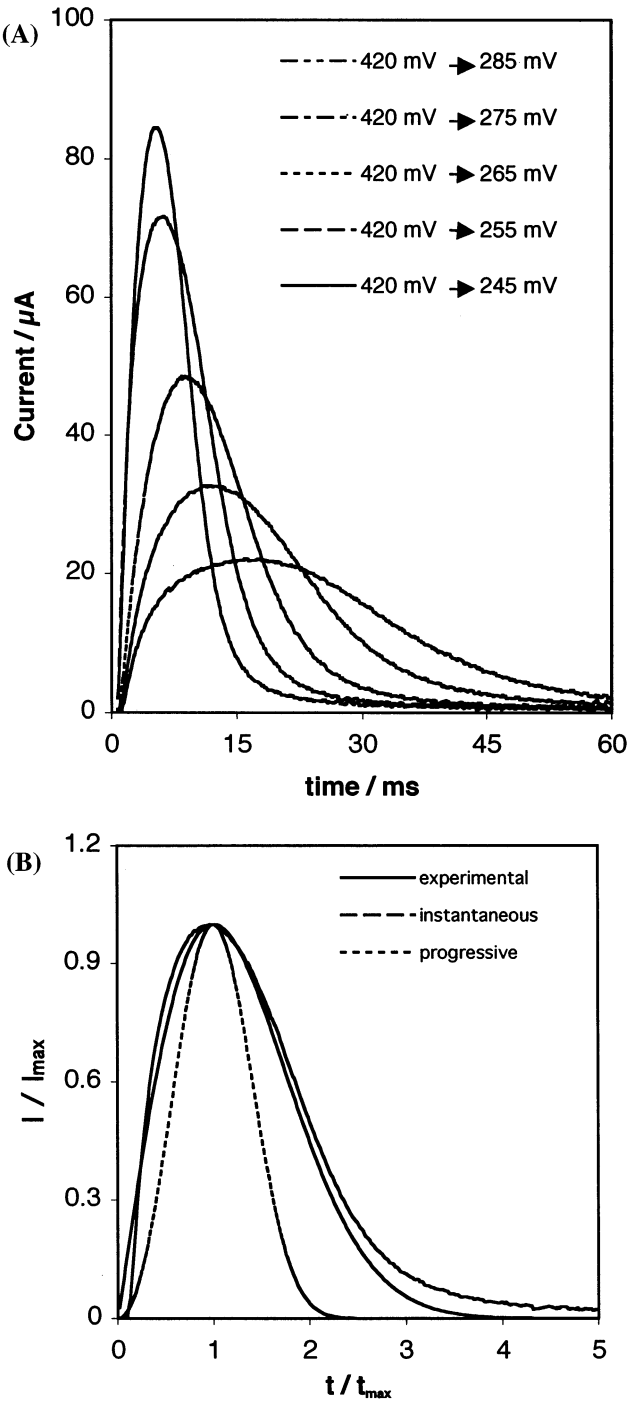

Figure 2. (A) Experimental current−time transients for potential steps through peak C1. The initial potential was 0.420 V in all cases, and the final (step) potential was varied from 0.240 to 0.285 V. The nonfaradaic charging currents obtained under the identical conditions in the absense of TeO_2 have been subtracted from these data. (B) Representative reduced variable plot showing excellent fit to instantaneous nucleation model. The potential step was from 0.420 to 0.255 V.

at potentials positive of the voltammetric peak suggests a complex or multistep deposition mechanism. One possibility is the expulsion of specifically adsorbed anions (or nonadsorbed anions near the inner Helmholz plane) in parallel with the reduction of $HTeO_2^+$. A reasonable mechanism would involve the loss of one specifically adsorbed ClO_4^- (MW ≈ 100 g/mol) from the surface as each $HTeO_2^+$ (MW ≈ 128 g/mol) was reduced to Te according to the equation

$$HTeO_2^+(aq) + 4e^- + 3H^+(aq) + ClO_4^-(ads) \rightarrow Te(ads) + 2H_2O(l) + ClO_4^-(aq) \quad (3)$$

If this mechanism were operative, it would mean that the mass gain of 128 g/mol associated with the deposition of Te would be accompanied by a mass loss of 100 g/mol associated with the expulsion of perchlorate. The overall process would still correspond to a net mass gain of ca. 28 g/mol, however, and is therefore inconsistent with our observation of a mass decrease. On the other hand, if $HTeO_2^+$ itself (or TeO_2, $HTeO_3^-$, etc.) were specifically adsorbed at potentials positive of peak C1, the reduction to Te would result in a net decrease in the mass because 2 mol of H_2O are liberated during the conversion of 1 mol of TeO_2 to Te. The mass loss expected for this process occurring at a 0.255 cm^2 surface area electrode is about 10 ng, which is in excellent agreement with our EQCM data. On this basis, we assign peak C1 to the following process

$$HTeO_2^+(ads) + 4e^- + 3H^+ = = = Te(ads) + 2H_2O(ads) \quad (4)$$

Although it has been shown by previous workers that $HTeO_2^+$ is the dominant species in solution at acidic pH's,[12] it should be noted that our experiments cannot distinguish between $HTeO_2^+$, TeO_3^{2-}, and TeO_2.[13] It should be noted that the adsorbed tellurite might not all be reduced. The question of what controls the extent of the reaction—the amount adsorbed, the surface area, or some other factor—remains unknown at this time.

To confirm that $HTeO_2^+$ is adsorbed at potentials positive of peak C1, we monitored the mass change at a Au electrode in pure $HClO_4$ electrolyte held at a potential of +0.700 V before and after the addition of an aliquot of TeO_2 (Figure 4). To rule out any possibility of the slow electrodeposition of Te in these experiments, we chose to work at a potential that was positive of the second UPD stripping peak (Figure 1, peak A2). The time-dependent EQCM data clearly show an increase in mass of about 20 ng over the course of about 1500 s, after which the signal saturates. This corresponds to a $HTeO_2^+$ coverage of 0.49 nmol/cm^2 and is in excellent agreement with the coverage of 0.41 nmol/cm^2 calculated independently from the charge under peak C1 assuming that the mechanism shown in eq 4 is valid. In addition, the presence of Te on the surface was confirmed by EDX measurements (data not shown). Because of the very limited solubility of TeO_2 in acidic aqueous solutions, the concentration of $HTeO_2^+$ is much lower for this experiment (on the order of micromolar) than is the case for the electrochemical measurements for which the formal concentration is 0.25 mM, and this helps to account for the slow adsorption behavior we observed. Finally, it is also important to note that, in all of our voltammetry and potential step experiments, the solutions were degassed for 20 min prior to making electrochemical measurements. Thus, we assume that the adsorption of $HTeO_2^+$ is complete prior to the first potential scan.

As mentioned earlier, the issue of TeO_2 adsorption at Au has not been completely resolved in the literature. Our results confirm the ex situ measurements of Stickney,[5] who claimed that oxidized Te is adsorbed at all potentials positive of the UPD potential, as evidenced by Auger electron spectroscopy. Yagi and co-workers[6] measured the potential-dependent SHG anisotropy of Au(111) electrodes in pure ClO_4^- electrolyte as well as in the presence of 0.5 mM TeO_2. Three lobes were observed in the SHG anisotropy in both cases, but there was a significant (ca. 60°) phase shift and intensity change in the signal

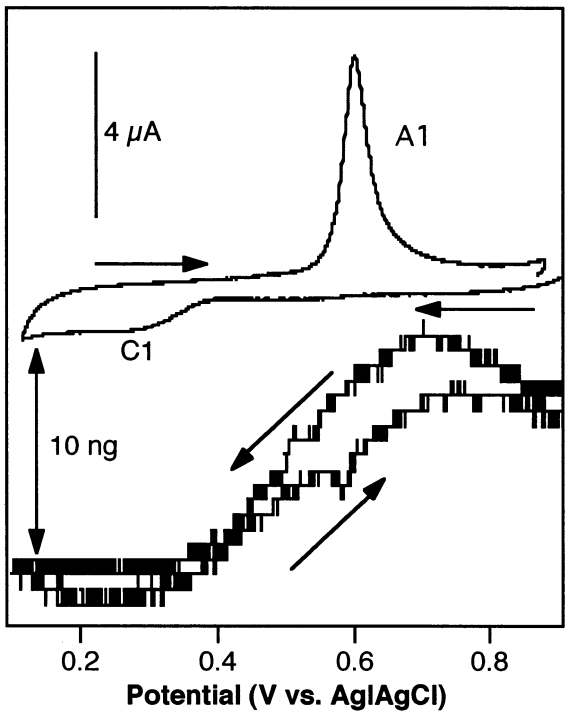

Figure 3. Cyclic voltammetry (CV) and in situ EQCM of peak C1. The lower trace shows Δmass vs potential data acquired in the UPD region near peak C1. The single-headed arrows indicate the scan direction. A mass decrease of approximately 10 ng is observed on the cathodic sweep, with a corresponding mass increase on the reverse (anodic) sweep. The upper trace shows CV data collected in parallel with the mass change data.

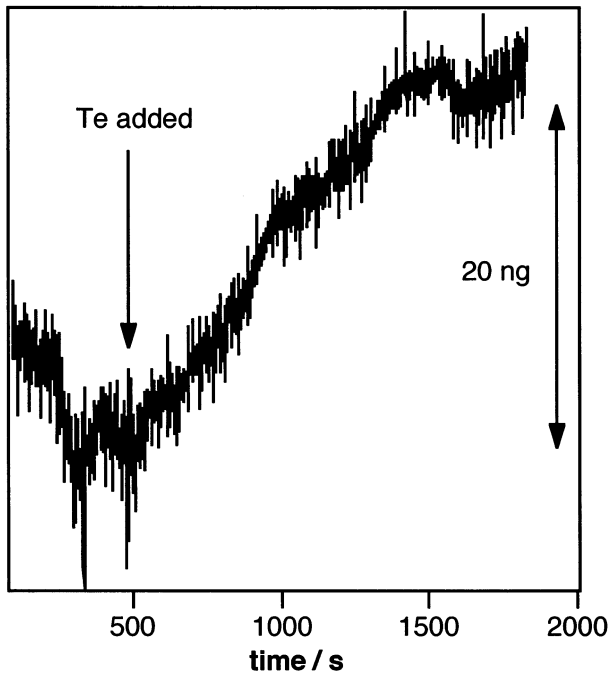

Figure 4. Δmass vs time plot for TeO_2 spiking experiment. A Au electrode was immersed in 0.10 M $HClO_4$ and poised at a potential of +0.700 V. After approximately 500 s, an aliquot of supporting electrolyte containing TeO_2 (saturated) was introduced. The mass increase of ca. 20 ng corresponds to a TeO_2 coverage of 0.49, in excellent agreement with the chronocoulometric coverage of 0.41.

as the potential was scanned through the first UPD wave (C1) in 0.5 mM TeO_2. On the basis of modeling studies, the SHG response appeared to be sensitive only to changes in the optical

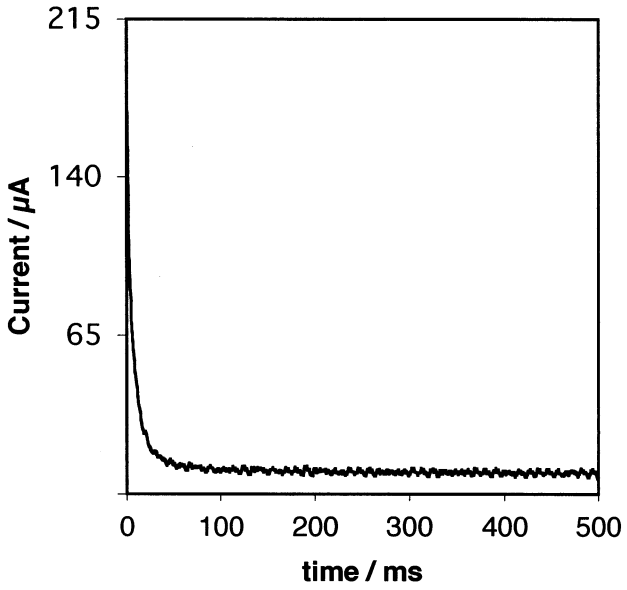

Figure 5. Experimental current−time transient for peak C2. The initial potential was +0.150 V, and the final (step) potential was 0.005 V. The exponential decrease of the current is consistent with Langmuir adsorption behavior.

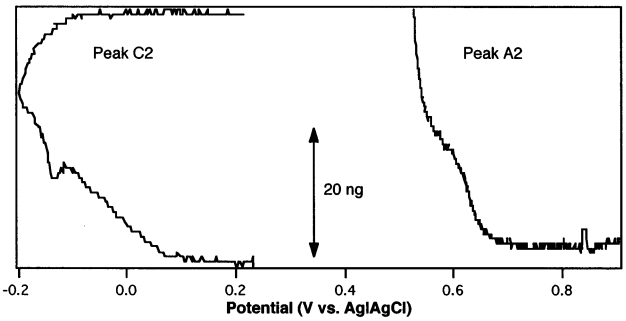

Figure 6. EQCM scans for peaks C2 and A2. The left-hand trace shows the Δmass vs potential data for the second UPD peak (C2). The deposition data indicate that Te UPD and bulk deposition occur in parallel near −0.150 V. The left-hand trace shows the Δmass vs potential data for the corresponding stripping wave (A2).

constants of the Au(111) surface itself, and not adsorbed Te. Indeed, the observed phase shift is not consistent with the Au-(111)($\sqrt{3} \times \sqrt{3}$)R30°−Te structure associated with peak C1. Stickney et al.[5] have also observed a restructuring of the underlying Au associated with Te UPD, and it might be that the SHG signal is more sensitive to the Au reconstruction than to the presence of adsorbed Te. In any event, the SHG experiments do not directly address the issue of preadsorbed TeO_2.

Peak C2. The second UPD wave occurs at a potential near −0.100 V vs Ag|AgCl. Current−time transients measured by stepping through this peak display a simple exponential decrease as a function of time with a total charge density of about 180 $\mu C/cm^2$ (Figure 5). This behavior is consistent with a Langmuir adsorption mechanism (i.e., simple chemisorption with no two-dimensional nucleation and growth) and likely corresponds to "filling in" of the monolayer after the reduction of adsorbed $HTeO_2^+$ and the concomitant loss of water from the surface. EQCM indicates a mass gain of approximately 15 ng for this process (Figure 6, left-hand trace). The EQCM data also show that there is significant overlap between UPD and bulk deposition, even though a distinct bulk deposition wave is not observed in the CV data. The small dip in the mass change

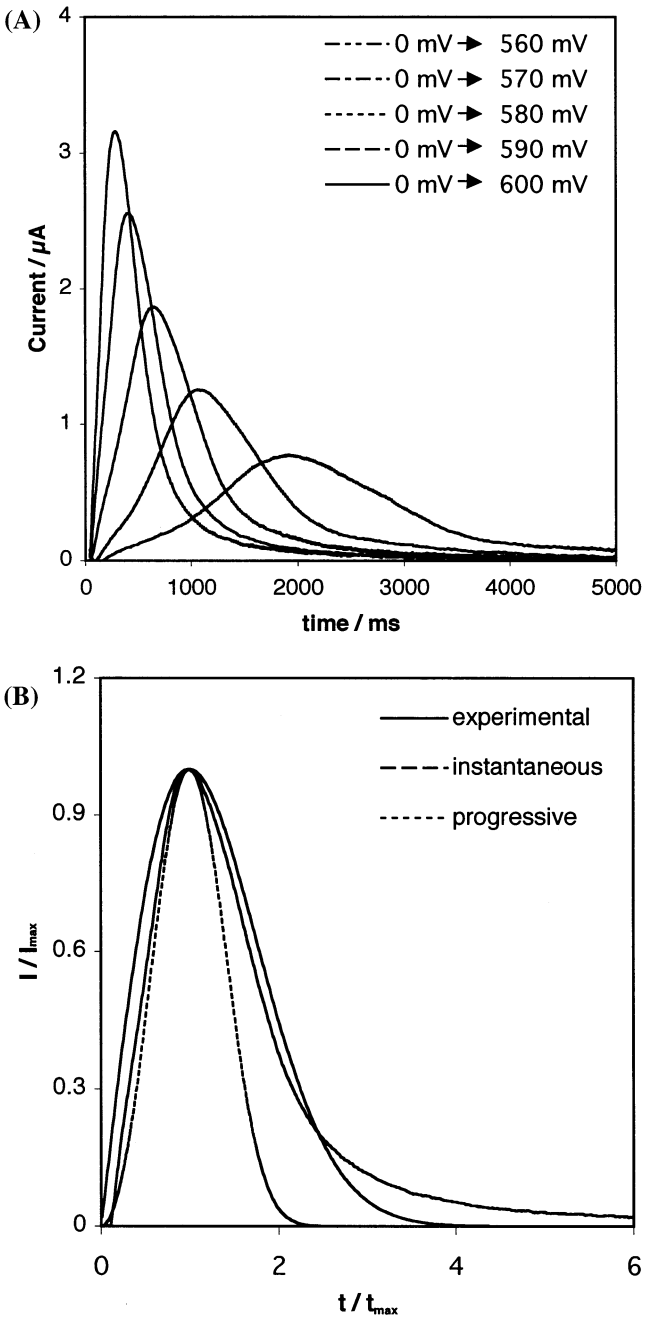

Figure 7. (A) Experimental current−time transients for potential steps through peak A1. The initial potential was 0.0 V in all cases, and the final (step) potential was varied from 0.600 to 0.560 V. The nonfaradaic charging current has been subtracted from these transients as with the data shown in Figure 2. (B) Representative reduced variable plot showing fit to instantaneous and progressive nucleation models. The potential step was from 0.0 to 0.560 V.

data that occurs at −0.150 V is always observed and indicates that UPD and bulk deposition are occurring in parallel at this potential. Evidence to support this interpretation comes from the observation that the mass change continues to increase even after the potential is switched at −0.2 V, which is indicative of a bulk deposition process. UPD, on the other hand, is a surface-limited reaction, and the associated EQCM signal is expected to go to zero as the potential is swept sufficiently negative. In addition, as the potential is swept back through −0.150 V on the anodic scan, the mass change goes to zero, which is also consistent with our interpretation. Because of the overlap of the UPD and bulk deposition waves, we cannot unambiguously

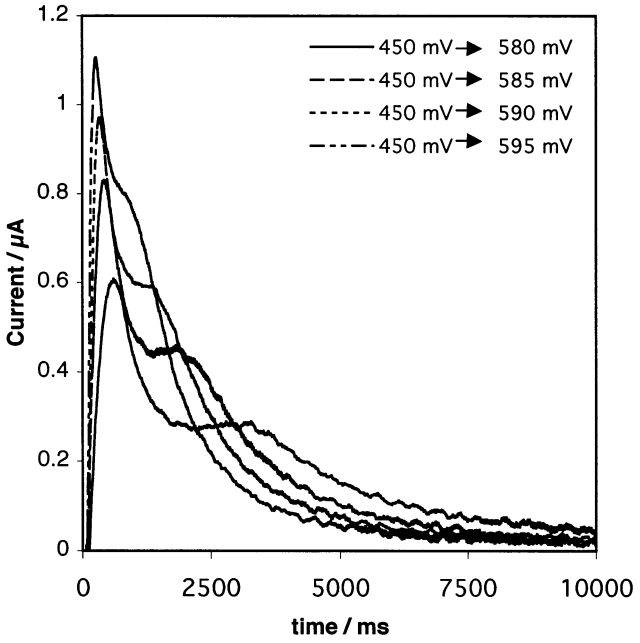

Figure 8. Experimental current−time transients for potential steps through peaks A1 and A2. The initial potential was 0.450 V in all cases, and the final (step) potential was varied from 0.580 to 0.595 V. The nonfaradaic charging current has been subtracted from these transients.

assign peak C2 as being associated with a specific structural phase transition as has been suggested by Sorenson et al.[5] These workers reported multiple ordered phases, as well as a roughening transition in the same general potential window as peak C2. After about 20−30 min, a pseudomorphic (1 × 1) structure was observed. On the other hand, Hayden et al.[7] reported only the pseudomorphic (1 × 1) structure. The EQCM data clearly show that more than one process is taking place in this potential region, at least at the polycrystalline surfaces examined in the EQCM experiments, and that a saturation coverage of approximately 0.9 is always observed. Analysis of the stripping waves provides more insight into the nature of the UPD phases that are formed.

Stripping Peaks (A1 and A2). Several general observations can be made with respect to the stripping behavior. First, the stripping processes both appear to be relatively slow compared to the corresponding deposition processes. For example, the initial UPD process occurs on a time scale of 10 ms, whereas stripping occurs on a 500-ms time scale. Similarly, peak C2 occurs on a time scale of 20 ms, whereas peak A2 occurs on a time scale of 2000 ms. It was possible to obtain current transients for the first stripping peak (A1) directly. The current time transients for peak A1 are shown in Figure 7A. These data could be fit reasonably well to an instantaneous 2D dissolution model especially at longer times (Figure 7B). We attempted to obtain current voltage transients for the second stripping feature, which was not possible because the two stripping peaks are so close together. However, we were able to deconvolve the two current voltage transients because the transient for the first stripping peak had been measured independently. Current-time transients for potential steps through peaks A1 and A2 are shown in Figure 8. Both stripping events proceed by what appears to be an instantaneous nucleation and growth mechanism (not shown). This behavior strongly supports the assertion by Sorensen et al. that the second UPD peak corresponds to a first-order phase transition between two stable structures. The deposition traces were not sensitive to this because of the overlap of peak C2 and the bulk deposition wave (i.e., UPD and bulk deposition

occur in parallel). In addition, the formation of these ordered phases might be kinetically slow. It is likely that the thermodynamically favored structure is the pseudomorphic (1×1) phase observed by both Sorensen et al. and Hayden et al. Mass change data show that the second UPD stripping peak corresponds to a mass change of about 15 ng (Figure 6, right-hand trace).

Finally, the sluggish stripping kinetics reflects the fact that the half reaction is termolecular; that is, an adsorbed Te atom must combine with two H_2O molecules to form $HTeO_2^+$. Nevertheless, both of these processes are rapid on the time scale of the linear potential sweep used in our CV and EQCM experiments. Thus, the large peak separation between the deposition and stripping peaks appears not to be a kinetic overpotential but to reflect the energetics of Te nucleation on Au surfaces.

Conclusions

We have characterized the UPD of Te on Au(111) surfaces using chronocoulometry and EQCM. Our results demonstrate unambiguously that the first UPD peak corresponds to the reduction of a preadsorbed layer of $HTeO_2^+$ to form Te and that the second UPD peak corresponds to the reduction of $HTeO_2^+$ from solution. In both cases, the half reaction appears to be the four-electron reduction of $HTeO_2^+$ to Te.

Acknowledgment. C.S. and I.N. acknowledge the financial support of the Petroleum Research Fund, the U.S. Department of Energy and the National Science Foundation. U.D. acknowledges the financial support of TUBITAK, the National Science Foundation of Turkey.

References and Notes

(1) Sapp, S. A.; Lakshmi, B. B.; Martin, C. R. *Adv. Mater.* **1999**, *11*, 402.

(2) Stickney, J. L. *Electroanal. Chem.* **1999**, *21*, 75.

(3) Shannon, C.; Gichuhi, A.; Barnes, P. A.; Bozack, M. J. *Proc. Electrochem. Soc.* **1999**, *99-9*, 282.

(4) (a) Feliu, J. M.; Llorca, M. J.; Gomez, R.; Aldaz, A. *Surf. Sci.* **1993**, *297*, 209. (b) Herrero, E.; Rodes, A.; Perez, J. M.; Feliu, J. M.; Aldaz, A. *J. Electroanal. Chem.* **1996** *412* 165. (c) Herrero, E.; Llorca, M. J.; Feliu, J. M.; Aldaz, A. *J. Electroanal. Chem.* **1995**, *383* 145. (d) Gregory, B. W.; Norton, M. L.; Stickney, J. L. *J. Electroanal. Chem.* **1990**, *293*, 85. (e) Suggs, D. W.; Stickney, J. L. *J. Phys. Chem.* **1991**, *95*, 10056. (f) Yagi, I.; Lantz, J. M.; Nakabayashi, S.; Corn, R. M.; Uosaki, K. *J. Electroanal. Chem.* **1996**, *401*, 95. (g) Yagi, I.; Nakabayashi, S.; Uosaki, K. *Surf. Sci.* **1998**, *406*, 1. (h) Suggs, D. W.; Stickney, J. L. *Surf. Sci.* **1993**, *290* 375. (i) Ikemiya, N.; Yamada, K.; Hara, S. *J. Vac. Sci. Technol.* **1996**, *B14*, 1369. (j) Ikemiya, N.; Iwai, D.; Yamada, K.; Vidu, R.; Hara, S. *Surf. Sci.* **1996**, *369*, 199. (k) Sorenson, T. A.; Lister, T. E.; Huang, B. M.; Stickney, J. L. *J. Electrochem. Soc.* **1999**, *146*, 1019.

(5) Sorenson, T. A.; Varazo, K.; Suggs, D. W.; Stickney, J. L. *Surf. Sci.* **2001**, *470*, 197.

(6) Yagi, I.; Nakabayashi, S.; Uosaki, K. *J. Phys. Chem. B* **1998**, *102*, 2677.

(7) Hayden, B. E.; Nandhakumar, I. S. *J. Phys. Chem. B* **1997,** *101*, 7751.

(8) Sauerbrey, G. *Z. Phys.* **1959**, *155*, 206.

(9) (a) Bosco, E.; Rangarajan, S. K. *J. Chem. Soc., Faraday Trans. 1* **1981**, *77*, 1673. (b) Bosco, E.; Rangarajan, S. K. *J. Electroanal. Chem.* **1981**, *129*, 25. (c) Bhattacharjee, B.; Rangarajan, S. K. *J. Electroanal. Chem.* **1991**, *302*, 207.

(10) Budevski, E. B. In *Comprehensive Treatise of Electrochemistry*; Conway, B. E., Bockris, J. O'M., Yeager, E., Kahn, S. U. M., White, R. E., Eds.; Plenum Press: New York, 1983; Vol. 7, pp 399−450.

(11) (a) Bewick, A.; Fleischmann, M.; Thirsk, H. R. *Trans. Faraday Soc.* **1962**, *58*, 2200. (b) Fleischmann, M.; Thirsk, H. R. In *Advances in Electrochemistry and Electrochemical Engineering*; Delahay, P., Tobias, C. W., Eds.; Wiley Interscience: New York, 1963; Vol. 3, p 123.

(12) Lepiller, C.; Cowache, P.; Guillemoles, J. F.; Gibson, N.; Ozsan, E.; Lincot, D. *Thin Solid Films* **2000**, *361*, 118.

(13) Thus, we cannot rule out a possibility such as $HTeO_2^+(ads) + 4e^- + 3H^+ = = = Te(ads) + 2H_2O(ads)$.